8-27-2012

Experimental study of electrostatic aerosol filtration at moderate filter face velocity

Andres Sanchez

Andres Sanchez
Candidate

Chemical and Nuclear Engineering
Department

This thesis is approved, and it is acceptable in quality and form for publication:

Approved by the Thesis Committee:

Dr. Timothy L. Ward , Chairperson

Dr. Heather Canavan

Dr. Joshua A. Hubbard

EXPERIMENTAL STUDY OF ELECTROSTATIC AEROSOL FILTRATION AT MODERATE FILTER FACE VELOCITY

by

ANDRES SANCHEZ

CHEMICAL ENGINEERING, BACHELORS OF SCIENCE
2008

THESIS

Submitted in Partial Fulfillment of the
Requirements for the Degree of

MASTERS OF SCIENCE
CHEMICAL ENGINEERING

The University of New Mexico
Albuquerque, New Mexico

JULY, 2012

Acknowledgements

I would like to thank my mentor Dr. Joshua A. Hubbard, from Sandia National Laboratories, for all his time and encouragement throughout my Master's program. I would also like to thank my academic advisor Dr. Timothy L. Ward, Chemical and Nuclear engineering department chair, for his support and help with final revisions on my manuscript. In addition, I would like to thank Jennifer Dellinger for her financial support and Brandon Servantes for his help with mechanical design and instrumentation.

Experimental Study of Electrostatic Aerosol Filtration at Moderate Filter Face Velocity

By

Andres Sanchez

B.S., Chemical Engineering, University of New Mexico, 2008

M.S., Chemical Engineering, University of New Mexico, 2012

ABSTRACT

Electrostatic filtration media (electret) has been used in many applications due to its ability to efficiently collect submicron particles while maintaining a low pressure drop. Filter face velocities have ranged from 0.01-0.5 m/s in previous studies. However, in this study, measurements were conducted from 0.5-2.5 m/s, a region where Reynolds numbers range from 0.05-0.24. Within this regime, commonly used filtration theory is incomplete and does not predict performance of electret media, therefore data must be measured. Experimental measurements were conducted in various combinations of charge and neutralized filter media with aerosolized particles possessing the Boltzmann charge distribution or zero charge. Collection efficiency of the charged Filtrete^{TM} media was significantly higher than the Filtrete^{TM} which had been charged neutralized. As filter face velocity increased, however, collection efficiency decreased in the electret media. As filter face velocity increased for the neutralized media, collection efficiency increased due to inertial impaction. Particle bounce was assumed to occur with particles of aerodynamic diameter $\geq$ 400 nm. Electrostatic attraction, i.e. Coulombic, polarization and image forces were analyzed based on

experimental data. The Coulombic force had the greatest effect on efficiency at all three filter face velocities, followed by the polarization force. The effect of image forces was negligible for all three filter face velocities. This study provides unique empirical data outside of the viscous filter flow regime, data which is useful in the design of, and performance prediction of, high volume commercial and industrial applications, such as HVAC (heating, ventilation, and air conditioning) systems. The data presented can be used to “validate” numerical models for filtration at moderate Reynolds numbers where data is scarce for electrostatically charged filtration.

Table of Contents

List of Figures

List of Tables

Nomenclature

A	Cross-sectional area of tube
$\bar{C}_d$	Aerosol concentration downstream (#/cm^3)
$\bar{C}_u$	Aerosol concentration upstream (#/cm^3)
C_c	Cunningham slip correction factor
D	Diameter of the filter
D_p	Particle Diffusion Coefficient (m^2/s)
d_a	Aerodynamic diameter (m)
d_f	Fiber diameter (m)
d_m	Electrical mobility diameter (m)
d_p	Particle diameter (m)
d_{ve}	Volume equivalent diameter (m)
E	Aerosol collection efficiency
e	Charge of electron (1.6E-19 C)
E	Electrical field strength
F_G	Gravitational force
L	Length (m)
l_e	Fiber equivalent length (m)
M	Molar
n	Number of elementary charges
nm	Nanometer
$\bar{P}_d$	Average air pressure downstream (Pa)
$\bar{P}_u$	Average air pressure upstream (Pa)
Q_A	Air flow at injection site (SLPM)
Q_S	Air flow at inlet of the filter test bed system (SLPM)
Q_T	Total air flow (SLPM)
R	Function of independent variables
r	Radius (m)
Re	Reynolds number
SA	Surface area (m^2)
Stk	Stokes number
t	thickness (μm)
U_{air}	Bulk gas velocity (m/s)
V	Filter face velocity (m/s)
V_f	Fiber volume (m^3)
V_T	Total filter volume (m^3)
V_{TE}	Terminal electrical drift velocity (m/s)
w_A	Aerosol generator uncertainty (LPM)
w_R	Result uncertainty
w_{Re}	Reynolds number uncertainty
w_S	TSI 4040-flowmeter uncertainty (LPM)
w_V	Velocity uncertainty (m/s)
α	Fiber Solidity
η	Dynamic viscosity (Pa·s)
λ	Mean free path
μm	Micrometer

ρ	Air density of filter test bed system (kg/m^3)
ρ_o	Standard density (kg/m^3)
ρ_p	Particle density (kg/m^3)
χ	Dynamic shape factor

APS	Aerodynamic Particle Sizer
ARD	Arizona Road Dust
BET	Brunauer, Emmett, and Teller
BMF	Blown micro-fiber
CPC	Condensation Particle Counter
DMA	Differential Mobility Analyzer
ESP	Electrostatic Precipitator
FTB	Filter Test Bed
HEPA	High Efficient Particle Air
LPM	Liters Per Minute
OD	Outer Diameter
PSIA	Pounds per Square Inch Absolute
PSIG	Pounds per Square Inch Gauge
RPS	Revolutions Per Second
SEM	Scanning Electron Microscope
SLPM	Standard Liters Per Minute
SMPS	Scanning Mobility Particle Sizer
SS	Stainless Steel

1. Introduction

Fine particles with aerodynamic diameters of < 3μm have been a great concern for many years due to their ability to penetrate into the human airways, as well as their prolonged atmospheric residence times (Cohen, Xiong, Fang, & Li, 1998; Henry & Ariman, 1981). Because submicron particles can rapidly transport through the human airways into the lower lung, there are studies that indicate that exposure could lead to pulmonary disease, cardiovascular health effects, and immune system impairments (Huang, Chen, Chang, Lai, & Chen, 2007). Electrostatic filtration media (electret media) has been used in many applications due to its enhanced collection efficiency for submicron particles while maintaining a low pressure drop. These conditions are ideal for respirators, clean rooms, or processing of nuclear and hazardous materials (Barrett & Rousseau, 1998; Brown, 1993; Fjeld & Owens, 1988; Hinds, 1999; Huang et al., 2007; C. S. Kim, Bao, Okuyama, Shimada, & Niinuma, 2006; Lathrache & Fissan, 1987; Lee, Otani, Namiki, & Emi, 2002; Wang, 2001).

Electrostatic filtration media has been the focus of many studies. Lathrache and Fissan (1986) studied the collection efficiency of electrostatically charged filters in comparison to theory in the viscous flow regime. In their study, they found that measured collection efficiency and theoretical data matched well; however, assumptions were made about fiber charge density of the fibers in order to match theory to data collected. Fjeld and Owens (1986) conducted a similar experiment under the same filter face velocity and found that measured penetration values were significantly higher than those predicted by theory. A similar conclusion was found in the work of Lee (2002) where high-performance electret fibers were used under viscous flow conditions. Lee found that theoretical models did not

match experimental data because of a significant increase in charge density (2002). Higher fiber charge density has been seen to decrease filter penetration (Wei, 2006). In addition to consistencies in fiber charge density, Martin (2000) described collection efficiency of various respirators made of electret media in the viscous flow regime and indicated that there is a real concern in the work environment since filter media can lose its electrostatic charge. Shaffer (2010) also indicated that there was a great need for additional research in the work place because there were limited studies with particles less than 100 nm which are often difficult to compare. Due to inconsistencies among electrostatic filters (e.g., solidity, fiber charge density, etc.), generalizations about electret media as a whole are difficult (Barrett, 1998).

Typical filter face velocities for electrostatic media have ranged from 0.01-0.5 m/s (Barrett & Rousseau, 1998; Fjeld & Owens, 1988; Huang et al., 2007; C. S. Kim et al., 2006; Shaffer & Rengasamy, 2009; Wang, 2001; Wei, Chun-Shun, & Cheong-Ki, 2006). In this study, however, velocity ranged from 0.5 to 2.5 m/s. This range is useful for high volume filtration such as HVAC systems. Contemporary filtration theory is based on the Kuwabara flow field which describes air flow streamlines through a staggered array of fibers where viscous flow is assumed. However, as flows approach the viscous-inertial transition regime theoretical models based on viscous flow begin to break down (Brown, 1993; Hinds, 1999). The relative importance of viscous and inertial forces is given by fiber Reynolds number (Re_f), defined as

$$Re_f = \frac{\rho V d_f}{\eta}. \qquad [1]$$

In equation [1], ρ is the air density in the filter test bed system, d_f is the diameter of the fiber, and η is the dynamic viscosity of air at standard temperature. Viscous flow is defined as $Re_f << 1$ where viscous forces dominate. Viscous forces are negligible for $Re_f >> 1$ which is

called potential flow. As filter face velocity increases, inertial forces become more important where the inertial force is just as important as the viscous force at $Re_f = 1$. The purpose of this work was to experimentally study total electrostatic filter efficiency at moderate filter face velocities where $0.05 < Re_f < 0.24$. In this filtration regime, very little experimental data is available and the accuracy of analytical theories is questionable.

2. Filter Test Bed

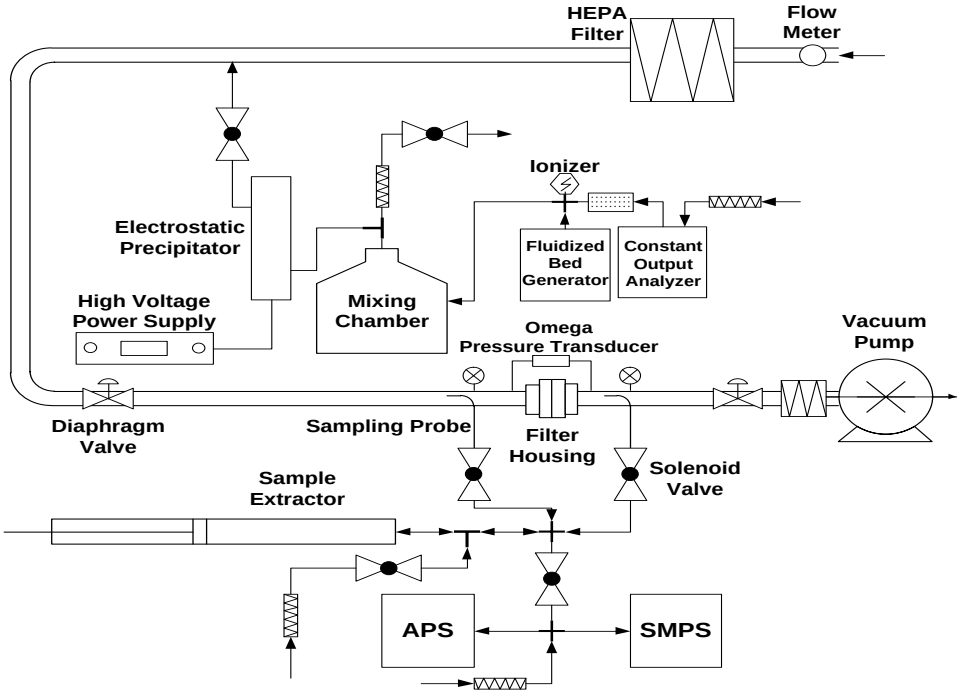

Figure 1: Filter Test Bed System (Schematic modified from Hubbard et al. 2012)

The filter test bed system, constructed by Hubbard et al., was used to study filtration in the viscous-inertial transition flow regime. For this study, the system was modified to measure electret filter media efficiency at non-traditional face velocities. Figure 1 above is a schematic of the modified filter test bed system.

This particular system was run at filter face velocities of 0.5, 1.5, and 2.5 meters per second (m/s), an air pressure of 0.8 atmospheres (atm), and at standard temperature (20 ^{o}C).

Air at atmospheric conditions was drawn in through a Model 4040- flow meter (TSI Inc. Shoreview, Minnesota, USA) and filtered using a 1'x1' square High-Efficiency Particulate Air (HEPA) filter. This process ensured that all air flowing through the system was clean prior to each test. The filtered air then flowed through a 2 inch stainless steel tube where test aerosol was injected. Flow was measured with the TSI flow meter and adjusted with a diaphragm valve located just before the filter housing. The system was kept at approximately 11.76 psia or 0.8 atm upstream of the filter using a rotary vane vacuum pump (Travaini Pumps USA, Inc., Yorktown, Virginia, USA). Pressure drop through the filter media was measured using a Model PX277-30D5V Omega Pressure Transducer (Omega Engineering, Inc. Stamford, Connecticut).

Two test aerosols, varying in size, shape, and density, were generated during these experiments. A $1.7x10^{-3}$ Molar (M) sodium chloride (NaCl) solution (Crystalline/Certified ACS, Fisher Chemical, S271-3) was aerosolized using a Model 3076- Constant Output Atomizer with a desiccant drier (TSI, Inc.).The constant output atomizer, Figure 2, generates liquid droplets from the NaCl solution that evaporate as they pass through the desiccant drier, leaving only a solid test aerosol. The constant output atomizer was used in the recirculation mode, where the 1-liter bottle with a protective plastic covering acts as the reservoir for the solution.

Figure 2: Image of TSI Constant Output Analyzer

Clean Compressed air was fed into the atomizer block, Figure 3, at 30 psig. As air enters into the atomizer block, it expands through and orifice to form a high velocity jet. At the same time, solution is drawn into the atomizing section from a 1/16th inch line from the 1-liter bottle and is atomized by the jet. Large droplets impact on the atomizing block wall and are drained back into the reservoir (TSI, 2005). The remaining fine spray leaves the top of the atomizer at 3-3.5 Liters per minute (LPM). The spray flows through a diffusion dryer filled with silica beads at the tube's outer wall where the solvent evaporates leaving solid aerosol particles.

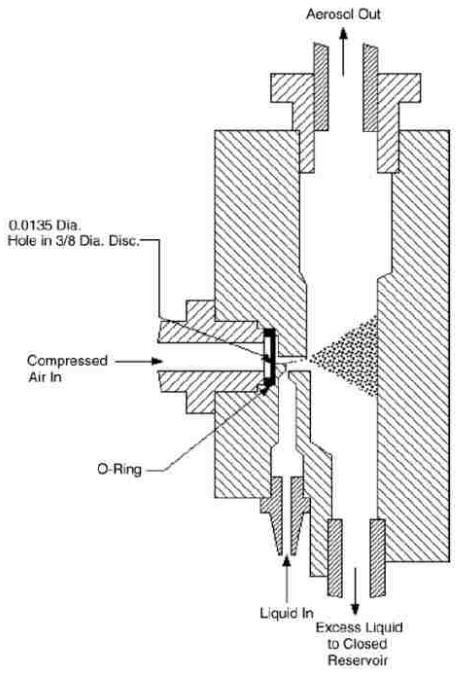

Figure 3: Model 3076 Schematic of the Atomizer Assembly Block (Image taken from TSI Inc. Constant Output Atomizer: Instruction Manual, P/N 1933076)

The second test aerosol was dispersed in powder form as fine Arizona Road Dust (ARD) (Powder Technologies Inc., South Burnsville, MN USA). It was aerosolized using a Model 3400A- Fluidized Bed Aerosol Generator (TSI, Inc.) as seen in Figure 4. The system

air pressure was set to 30 psia and drawn through a HEPA filter connected to the back panel. It was important to have a clean air source for the fluidized bed to prevent ambient aerosol particles from entering into the test system. Bead purge airflow was set at 5 LPM, bed airflow was set at 20 LPM, and bead speed was set at 30%. Average air flow rate by the fluidized bed was 12 ± 3 LPM.

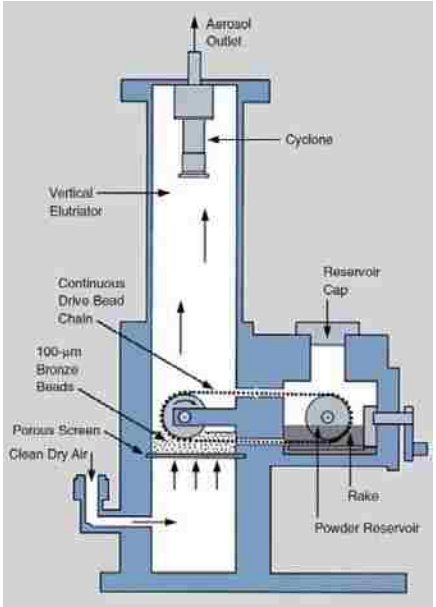

Figure 4: Model 3400A Schematic of Fluidized Bed Generator (Image obtained from TSI Inc.)

The TSI constant output atomizer and fluidized bed were run independently. After each aerosol was generated, it entered into a 5 liter mixing chamber (Spraying Systems Co., Wheaton, Illinois, USA) which had two outlet ports that were controlled by two separate pneumatically actuated ball valves. The first port was connected to a HEPA filter and vented outside the filter test bed, allowing the system to be run continuously without unnecessary filter loading. A single point ionizer (Haug Static Control Products, Williamsville, New York, USA) was connected to the second port in order to electrostatically charge neutralize the particles into the Boltzmann equilibrium charge distribution. This is where the charge distribution has an equal number of positively and negatively charged particles and is

therefore symmetric around zero (Hinds, 1999). This represents the charge distribution of an aerosol in charge equilibrium with bipolar ions. After passing through the single point ionizer, the aerosol entered into an electrostatic precipitator, which was constructed for these experiments. The electrostatic precipitator will be discussed in detail in the next subsection.

Aerosol samples were extracted isoaxially with sampling probes upstream and downstream of the filter housing in which the flow in the sampler inlet is moving in the same direction as the flow being sampled. T-type thermocouples and pressure transducers (Model PX277-30D5V, Omega Engineering, Stamford, CT USA) were placed in-line with the sampling probes. The Omega pressure transducer measured the pressure drop across the filter and provided a measurement of aerosol loading. It was calibrated by Omega prior to the first set of experiments for accuracy. A two liter extraction piston assembly was mounted to a linear ball screw and stepper motor. Pneumatically controlled ball valves were used to switch the extractor piston port among upstream sampling probe, downstream sampling probe, instrumentation delivery line, and filtered air for pressure equilibrium (Hubbard et al., 2012). Samples were drawn into the piston from the sampling ports at system pressure and extraction speed of 0.95 Revolutions Per Second (RPS), then brought to atmospheric pressure by bleeding in HEPA filtered air. Atmospheric pressure was required for the Aerosol Particle Sizer (APS-Model 3321, TSI Inc.) and the Scanning Mobility Particle Sizer (SMPS, TSI Inc.). Extracted particle concentration was unaffected by the additional air to equilibrate the pressure because it is a constant volume sampling procedure (Hubbard et al., 2012).

The extraction speed (RPS) was specified to obtain an isokinetic extraction velocity of 2.5 m/s. Isokinetic sampling ensures that the air stream entering the collector has a velocity equal to that of the air in the gas stream just ahead of the sampling port (Hinds,

1999). Two test velocities, 0.5 and 1.5 m/s, were super-isokinetically sampled, where the velocity in the probe exceeds the stream velocity, to avoid extended time within the sampling tube, which could cause diffusion losses for particles in the nanoparticle range (<100 nm). Super-isokinetic sampling of supramicron particles did not result in sampling biases because efficiency calculations only take into consideration the difference in the upstream and downstream measurements (both were extracted in the same fashion). Inertial losses due to super-isokinetic sampling were calculated and negligible for particle sizes less than 2 micrometers (μm) (Baron & Willeke, 2001).

The APS was used to measure particles with aerodynamic diameters from 0.5 to 20 μm at a sampling air flow rate of approximately 5 ± 0.2 LPM. In this study, the APS was primarily used for measurement of Arizona Road Dust (ARD). An SEM image of ARD can be seen in Figure 5 below. The APS uses time-of-flight particle sizing technology, in real time, to measure acceleration of aerosol particles in response to the accelerated flow of the sample aerosol through a nozzle (TSI, 2002). Time of flight uses two narrowly focused laser beams to determine an average particle velocity between a timing zone. A large or heavier particle will lag behind the air and will have a lower velocity in the timing zone. The magnitude of this lag, along with a suitable calibration, determines the aerodynamic particle diameter (Hinds, 1999).

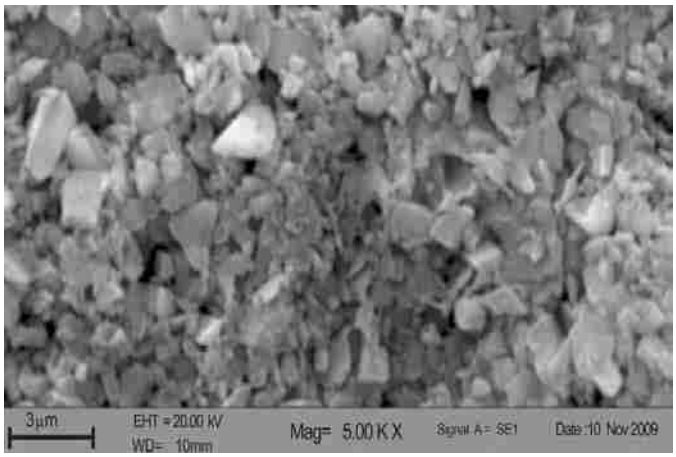

Figure 5: SEM Image of ARD. (Image taken from Helgeson, 2011)

The SMPS system was primarily used to measure NaCl particles with electrical mobility diameters between 10 and 500 nm with a set sheath flow of 5.0 ± 0.05 LPM and sample flow rate of 0.5 LPM. Flow rates were set to attain a 10:1 ratio of sheath air to aerosol sample to achieve the best resolution (TSI, 2003). The SMPS system is a combination of two TSI instruments: a series 3080- Electrostatic Classifier with a series 3081-Long Differential Mobility Analyzer (DMA) that size classifies particles, and a series 3785 Water-based Condensation Particle Counter (CPC) that measures aerosol number concentration. Figure 6, below, is an SEM image of the NaCl particles.

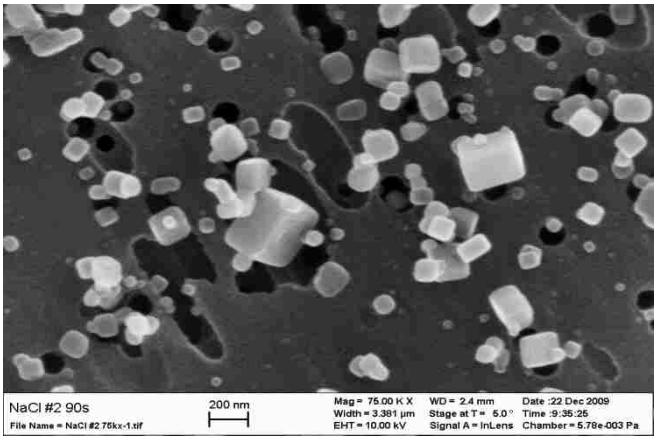

Figure 6: SEM Image of NaCl Particles

Polydisperse particles enter into the electrostatic classifier through an impactor to remove particles larger than 10μm that might cause data inversion problems (Hinds, 1999). The aerosol then enters a Kr-85 Bipolar Charger, which neutralizes particle charge, and flows into the DMA. The aerosol surrounds the inner core of sheath air, and both flows pass down the annulus with no mixing of the two laminar streams. The collector rod is maintained at a controlled negative voltage, while the outer cylinder is electrically grounded (TSI, 2003). Particles with greater mobility migrate to the central rod before reaching the gap located at the bottom of the collector, while those with lower mobility go beyond the gap and are filtered out. The exiting aerosol is nearly all singly charged and nearly monodisperse. At this point, the monodispersed aerosol enters into the water-based CPC where the particles grow due to condensation. Finally, the particle number concentration is measured using a light scattering technique. The DMA scans over a range of particle sizes resulting in a continuous particle size distribution.

2.1 Electrostatic Precipitator

The effects of particle charge on filter efficiency were measured. To do so, a simple electrostatic precipitator, Figure 7, was designed to remove all charged particles from entering into the filter test bed system. This was important to determine how collection efficiency of the Filtrete^{TM} media was affected by neutral particles at nontraditional filter face velocities. In previous studies, a particle with no charge of its own can develop an induced dipole when in the presence of electrically charged fibers, which will increase overall collection efficiency (Hinds, 1999). However, at higher face velocities, shorter residence times will affect electrostatic attraction (C. S. Kim et al., 2006). In this study, the electrostatic precipitator was only used for NaCl particles.

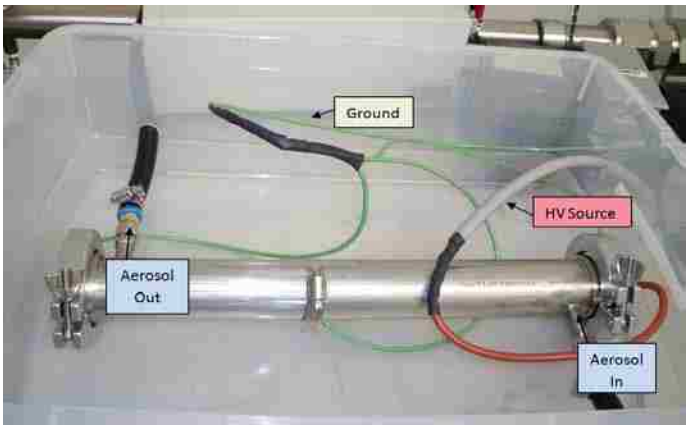

Figure 7: Image of Simple Electrostatic Precipitator with labels

The electrostatic precipitator (ESP) was designed with conservative dimensions (i.e. length) to ensure all charged particles were removed, leaving only particles with zero charge. A two inch outer diameter (OD) grounded stainless steel (SS) tube was used as the collection surface with a negatively charged copper rod located in the center. The charge difference creates an electric field perpendicular to the aerosol flow. As particles flowed through the electrostatic precipitator tube, positively charged particles were attracted to the negatively charged copper rod and negatively charged particles were attracted to the grounded stainless steel tube, allowing only neutral particles to flow out of the precipitator and into the filter test bed system, Figure 8. The copper rod was charged to -5000 Volts using a Bertan Series 225 High Voltage Power Supply (Spellman High Voltage Electronics Corporation, Hauppauge, NY USA). Voltage was adjusted to the highest level possible before arcing would occur inside the ESP. The copper rod was soldered to the high voltage source wire and isolated from the grounded SS tube with Teflon Swagelok bulkhead fittings. An inlet and outlet SS port was welded on opposite ends of the ESP for aerosol flow. The entire precipitator was placed into a plastic secondary container as an added engineering safety control.

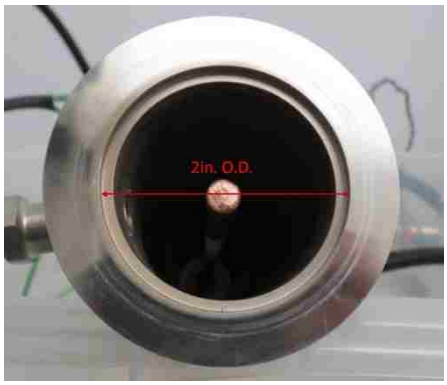

Figure 8: Side Image of ESP

The length of the electrostatic precipitator was determined using the following equation:

$$L = \frac{U_{air} \cdot r}{V_{TE}}, \qquad [2]$$

where U_{air} is the bulk gas velocity and r is the radius of the SS tube. V_{TE} is the terminal electrical drift velocity, which Brown et al. (1993) defined as the drift velocity of a particle under the influence of an electrical force. The terminal electrostatic velocity is defined in Hinds (1999) as:

$$V_{TE} = \frac{neC_c}{3\pi\eta d_p} E \, . \qquad [3]$$

In equation [3], n is the number of elementary charges on the particle, e is the charge of electron, C_c is the Cunningham slip correction factor, η is the viscosity, d_p is the particle diameter, and *E* is the electrical field strength. Figure 9 below is an illustration of the effect of terminal velocity on a single particle traveling in the direction of the air velocity (U_{air}).

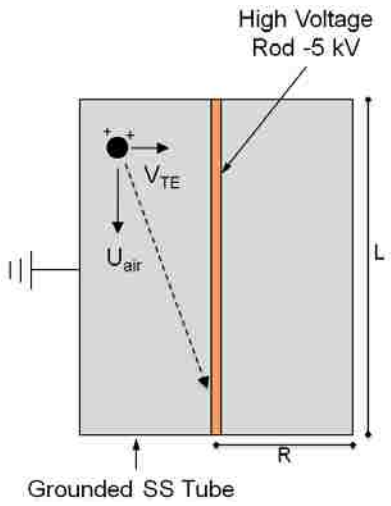

Figure 9: Visual representation of a charged particle in the ESP

In order to determine the minimum length required to collect all charged particles, calculations were performed using a particle with a single elementary charge. Particles with a higher charge would be removed at a shorter distance, therefore, the minimum length was determined with a singly charged particle, which would have the minimum terminal electrostatic velocity, i.e. longest distance to travel before collected. The minimum length was calculated as 14 inches, assuming a constant air flow of 3 LPM, particle size of 1μm, standard temperature and pressure, and set radius of 1 inch. A conservative length of 16 inches was used in the final design to ensure all charged particles were removed.

3. Experiment

3.1 Aerosol Particles

ARD and NaCl aerosols were sampled directly from the filter test bed with isoaxial sampling probes. Because the APS and SMPS systems use different particle size techniques, time-of-flight and electrical mobility, respectively, particle diameters were converted into a single coherent measure in order to have an accurate comparison of filter efficiency from the

two instruments. In this way, particle density and morphology can be taken into consideration. For this study, electrical mobility diameter, as measured with the SMPS system, was converted into aerodynamic diameter. The electrical mobility diameter of a particle is determined in comparison with the diameter of a sphere with the same terminal velocity in a constant electric field as the particle in question (DeCarlo, Slowik, & Worsnop, 2004). Aerodynamic diameter is defined as the diameter of the spherical particle with a standard density (ρ_o) of 1.0 g/cm^3 that has the same terminal settling velocity (V_{TS}) as the particle being measured (Hinds, 1999).

In order to convert electrical mobility diameter (d_m) to aerodynamic diameter (d_a), the volume equivalent diameter, d_{ve}, was calculated using the recursive equation

$$d_{ve} = d_m \frac{C_c(d_{ve})}{C_c(d_m)} \cdot \frac{1}{\chi}. \quad [4]$$

In equation [4], C_c is the Cunningham slip correction factor, where λ is the mean free path, and is defined as:

$$C_c = 1 + \frac{\lambda}{d}\left[2.34 + 1.05\, exp\left(-0.39\frac{d}{\lambda}\right)\right]. \quad [5]$$

This correction factor was derived for Stokes law to account for the effect of slip at the surface of the particle (Hinds, 1999). As the particle size (d) approaches the mean free path (λ) of air, the particle will slip through the air, thereby affecting particle drag. The second correction in equation [4] accounts for the increased drag on a particle due to non-spherical shape and is called dynamic shape factor (χ). Aerodynamic diameter decreases with increasing dynamic shape factor (DeCarlo et al., 2004). According to literature, the measured ρ_p for NaCl was 2.04 g-cm^{-3} and χ was 1.11 (Spencer, Shields, & Prather, 2007). These values will be used for the remainder of this study.

Volume equivalent diameter was then converted to aerodynamic diameter using the following recursive equation:

$$d_a = d_{ve}\sqrt{\frac{1}{\chi}\frac{\rho_p}{\rho_o}\frac{C_c(d_{ve})}{C_c(d_a)}}\,. \qquad [6]$$

This equation was derived by combining equations [7] and [8] below, where the terminal velocity is obtained when the gravitational force (F_G) is equal and opposite the drag force (DeCarlo et al., 2004).

$$F_G = \frac{3\pi\eta V_{TS} d_{ve}\chi}{C_c(d_{ve})} \qquad [7]$$

$$F_G = \frac{3\pi\eta V_{TS} d_a}{C_c(d_a)} \qquad [8]$$

In equation [7] and [8], η is the dynamic viscosity. In equation [8], $\chi = 1$. The recursive equations were solved using the engineering software MathCad. Figure 10 below is the calculated ratio of aerodynamic to electrical mobility diameter (d_a/d_m) for NaCl particles. This ratio shows that the aerodynamic diameter can be about 40 to 80% greater than electrical mobility diameter depending on the particle size. This figure confirms the importance of the particle diameter conversion, which is to accurately compare filter efficiency of ARD and NaCl on a consistent scale using two instruments with different particle size techniques.

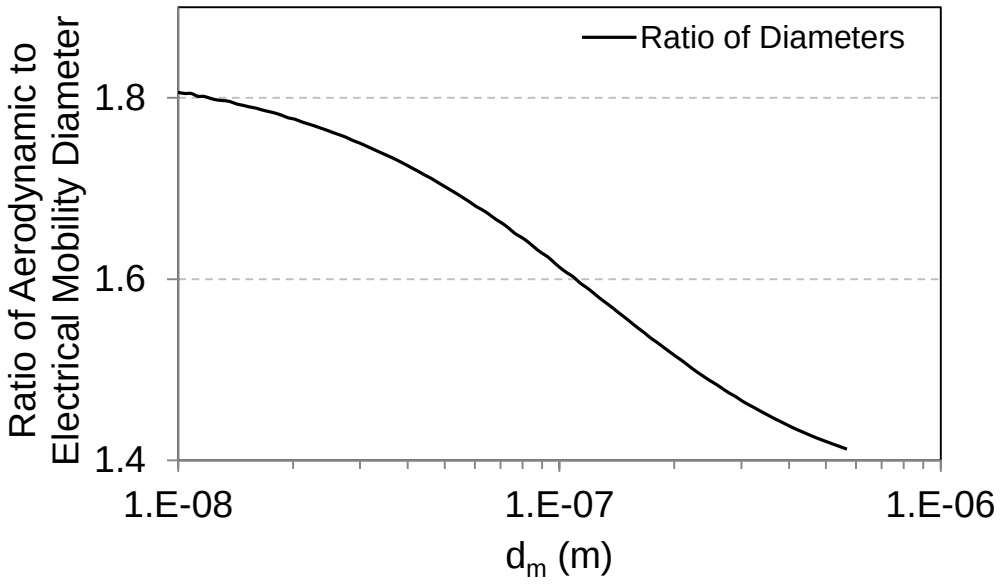

Figure 10: Graphical representation of aerodynamic to electrical mobility diameter ratio, where ρ_o is 1 g/cm^3, ρ_p for NaCl is 2.04 g/cm^3, and χ is 1.11according to Spencer, Shields, and Prather (2007)

3.2 3M Filtrete™

Aerosol collection efficiency of 3M Filtrete™ media, model BMF20F, was used in this study. Filtrete™ is an electret media, made of polypropylene, which uses electrostatically charged fibers to increase collection efficiency while maintaining a lower pressure drop than other filter media. This is important because it can be used in higher flow applications with lower power consumption (3M, 1993). Typical applications include respirators, home air purifiers, and clean rooms.

3M Filtrete™ consists of Blown Micro-Fibers (BMF) that satisfies HEPA performance standards. BMF is produced by blowing air, at high velocity, through an extruder die tip which carries a molten polymer onto a conveyor screen to form a fine self-bonding web. A Typar cover web, which provides mechanical stability for the filter, is connected to the top and bottom of the BMF electret. Figure 11, below, is a Scanning electron microscope (SEM) image of the Filtrete™ media at a width of 250μm. The large

fibers, at the left, are part of the Typar cover web and the smaller fibers are part of the BMF electret.

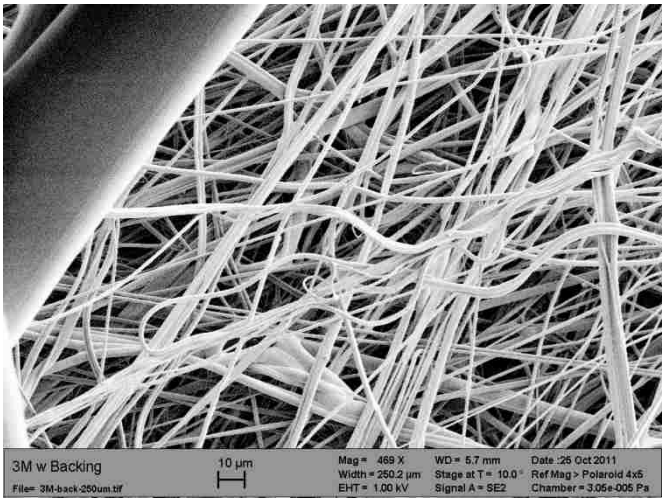

Figure 11: SEM image of 3M Filtrete™ at a width of 250µm

The fibers of electret media are electrostatically charged using corona discharge during the manufacturing process. This process emits ions using a point electrode, at a high potential, to create an electric field. These ions will drift due to the electric field and collect to a surface at lower potential, in this case the polypropylene fibers, and will develop a static charge (Brown, 1993). The polypropylene filters retain a line-dipole configuration with random orientation.

3.2.1 Physical Characterization

The following physical characteristics of the Filtrete™ media were measured: fiber diameter, thickness, and specific surface area. The Typar cover web was not taken into consideration since it is an insignificant source of particle collection. The average fiber diameter was calculated from SEM images. Ten random fibers were measured for three separate filter specimens. Analysis of these images was performed using the JAVA-based image processing program ImageJ (National Institute of Health, Bethesada, Maryland USA).

Average fiber diameter (d_f) was calculated at 1.77µm with a standard deviation of 0.33µm. Filter mat thickness (t) was measured using a Wyko NT9800 Optical Profiling System (Veeco, Plainview, NY USA). It is a 3-dimensional non-contact surface measurement instrument, which measures the topographical characteristics of a material from 0.1nm to 10 mm. This measurement technique was important to provide a very accurate thickness measurement without coming into contact with the surface of the material, which could bias the accuracy. Figure 12 is an example of the Wyko NT9800 X-Y scan in the Z direction. In the left figure, the red bar represents the scan in the X-direction (filter mat to the baseline thickness) and the blue bar is the scan in the Y-direction (filter mat only). The thickness was measured from the top, middle, and bottom of three filter pieces. The average thickness was 168.1µm with a standard deviation of 17.8µm.

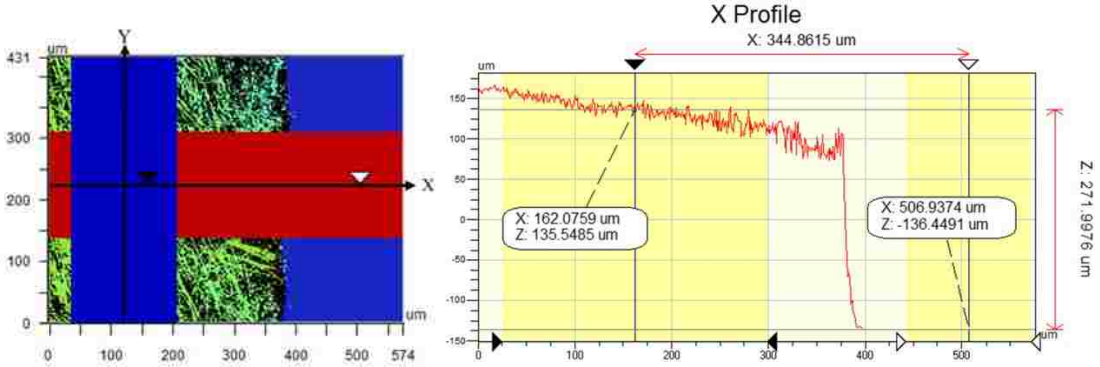

Figure 12: Wyko NT9800 X-Y Topographic Scan.

Specific surface area was measured using a TriStar 3000 V6.08A instrument (Micromeritics Instrument Corporation, Norcross, GA USA). This particular instrument uses BET (Brunauer, Emmett, and Teller) theory to determine specific surface area by describing adsorption of gas molecules, helium in this case, on a solid surface. The average specific

surface area was 1.747 ± 0.007 m^2/g. Specific surface area was used to determine fiber solidity, α, as defined by Hinds (1999),

$$\alpha = \frac{Fiber\ Volume}{Total\ Volume} = \frac{d_f^2 l_e}{D_f^2 t} \ , \qquad [9]$$

where fiber volume (V_f) is

$$V_f = \frac{\pi d_f^2}{4} l_e \ . \qquad [10]$$

In equation [10], l_e, is the fiber equivalent length or the length of a fiber if all fiber solids were made into a continuous strand (Bragg & Pearson, 1979). Fiber equivalent length is defined as

$$l_e = \frac{SA}{\pi d_f} \ . \qquad [11]$$

Surface area (SA) was calculated by multiplying the BET specific surface area by the average mass of a single filter, which was 0.065g. Surface area was calculated as 0.1136 m^2. Total filter volume (V_T) is

$$V_T = \frac{\pi D^2 t}{4} \ , \qquad [12]$$

where D is the cross-sectional diameter of the filter mat (0.06382 m). Solidity was calculated at 0.09 ± 0.01 , which is within the typical solidity of a fibrous filter of 0.01 and 0.3 (Hinds, 1999).

3.2.2 Charge Neutralization

The effect of fiber charge was studied by comparing the original collection efficiency of the Filtrete™ media to a charge neutralized version of the same media. This was important to differentiate collection efficiency of the filter from the traditional deposition mechanisms (interception, inertial impaction, diffusion, and gravitational settling) to electrostatic

attraction. Charge neutralization can occur by soaking the filters in various organic solvents including isopropanol, acetone, benzene, xylene, and ethyl-benzene (J. Kim, Jasper, Barker, & Hinestroza, 2010). Isopropanol (CAS 67-63-0, Fisher Scientific Inc., Pittsburgh, PA USA) was the solvent used in this work. According to various studies, the time the filter is exposed to the liquid solvent can vary from 15 seconds to 2 hours with no apparent difference in charge deterioration and no physical change in the polypropylene fibers (Huang et al., 2007; J. Kim et al., 2010; Martin & Moyer, 2000; Wei et al., 2006). A conservative approach of 1 hour isopropanol soak with a 24 hour dry time was used. Figure 13 below is an SEM image of the filter media after charge neutralization. There was no apparent change in the physical characteristics when fiber diameter measurements were compared to those from charged fibers, Figure 11.

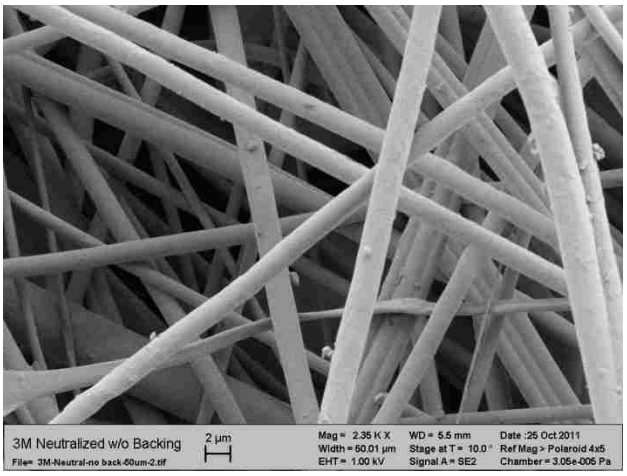

Figure 13: SEM image of 3M Filtrete^{TM} after charge neutralization at a width of 50µm

The reason fiber charge neutralization occurs has not been determined. There have been multiple theories of why this happens, including a chemical reaction between the filter and solvent, charge detrapping by solvent molecules, or plasticization, which is an increase in chain and charge mobility in the polypropylene fibers (J. Kim et al., 2010). Further research is needed to determine the exact cause.

3.3 Airflow Conditions

Average filter face velocities, Reynolds numbers (Re), and associated uncertainties were calculated for the filter test bed system. Total air flow rate (Q_T) in the filter section was calculated from the sum of the measured value at the inlet of the system, prior to the aerosol injection site (Q_S), and the air flow rate associated with the aerosol injection site (Q_A), see Figure 14. The total air flow rate is used to calculate the filter face velocity.

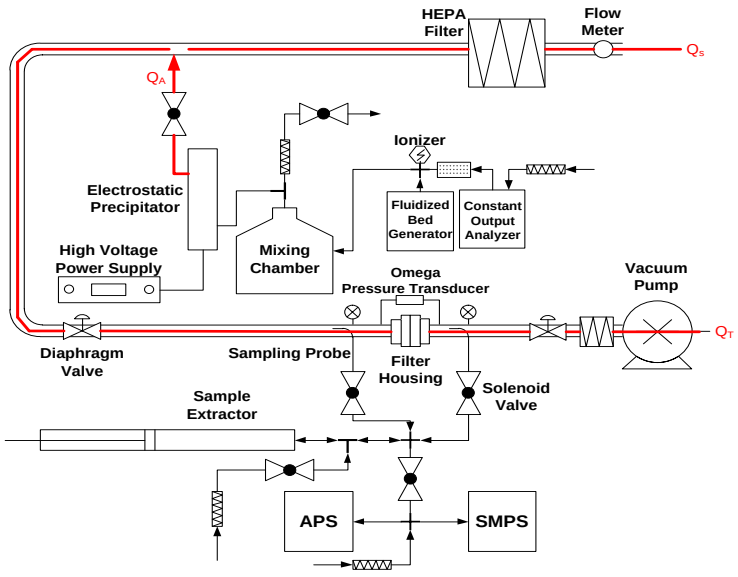

Figure 14: System Flow Diagram

Each aerosol generating device has a different air flow rate (Q_A) and uncertainty associated with it, which propagates into calculations of the filter face velocity and corresponding uncertainty.

3.3.1 Uncertainty Calculation

Uncertainty calculations are important for any study because measurement error propagates into calculations. In this study, uncertainty was determined for filter face velocity and Reynolds number due to uncertainties associated with flow rate calculations.

According to reliability estimates, there are two categories of experiments: single-sample and multiple-sample experiments (Kline & McClintock, 1953). Multiple-sample experiments base error on standard deviation of repeated measurements. When measurements cannot be repeated to determine uncertainty, it is called a single-sample experiment. For this study, filter face velocity and Reynolds number uncertainties were calculated assuming both single-sample and multiple-sample conditions. This was done to determine the greatest level of uncertainty.

Single-sample uncertainty analysis was described under the third theorem by Kline and McClintock in 1953 with the second-power equation:

$$w_R = \left[\left(\frac{\partial R}{\partial x_1} w_1\right)^2 + \left(\frac{\partial R}{\partial x_2} w_2\right)^2 + \cdots + \left(\frac{\partial R}{\partial x_n} w_n\right)^2\right]^{1/2} . \quad [13]$$

In equation [12], R is a function of independent variables (x_1, x_2, x_3,...,x_n) and w_R is the uncertainty in the result. For this study, filter face velocity was calculated using the following equation:

$$V = \frac{Q_T}{A} . \quad [14]$$

In equation [14], A is the cross-sectional area of the tube (1.64 x 10^{-3} m^2). Using equation [13] to solve for uncertainty in equation [15], the following equation was derived:

$$w_V = \left[\left(\frac{1}{A} w_S\right)^2 + \left(\frac{1}{A} w_A\right)^2\right]^{1/2} . \quad [15]$$

In equation [15], w_s is the uncertainty from the TSI 4040-flow meter and w_A is the uncertainty associated with either aerosol generator, which was, approximately, 0.5 LPM (8.33 x10^{-6} m^3/s) and 3 LPM (5 x 10^{-5} m^3/s) for the constant output atomizer and fluidized bed generator, respectively. Uncertainty for the constant output analyzer was determined from TSI documentation. Uncertainty for the fluidized bed was determined from a set of flow

measurements and estimated uncertainty from the bead purge and bed flow valves. The accuracy of the TSI 4040-flow meter was 1.75%, according to a calibration conducted by TSI Inc. on August 2011. Uncertainty of each filter face velocity using the single-sample approach is shown in Table (1).

Using the uncertainty from filter face velocity, uncertainty in the Reynolds number can be determined. Reynolds number is defined as:

$$Re_f = \frac{\rho V d_f}{\eta}. \quad [1]$$

In equation [1], ρ is the air density in the filter test bed system (0.96 kg/m^3), d_f is the diameter of the fiber (1.77 x 10^{-6} m), and η is the dynamic viscosity of air at standard temperature (1.836 x10^{-5} Pa·s). It was assumed that uncertainty from density, fiber diameter, and dynamic viscosity were minimal in comparison to uncertainty in the filter face velocity, therefore, uncertainty in the Reynolds number was calculated with equation [16], using equation [13]:

$$w_{RE} = \left(\frac{\rho d_f}{\eta} w_V\right). \quad [16]$$

Multiple-sample uncertainty was calculated at each filter face velocity with each aerosol generating device. Standard deviations at each flow rate were determined from 15 individual tests. Single- and multiple-sample uncertainty calculations of filter face velocity and Reynolds number at each filter face velocity can be seen in Table (1) and (2), respectively. According to the results, the highest level of uncertainty `came from single-sample uncertainty (i.e., uncertainty in flow rate measurement).

	Filter Face Velocity (m/s)	Single-Sample Uncertainty (m/s)	Reynolds Number	Single-Sample Uncertainty
Constant Output Atomizer	0.50	0.01	0.046	0.001
	1.50	0.03	0.139	0.002
	2.50	0.04	0.232	0.004
Fluidized Bed	0.65	0.03	0.060	0.003
	1.64	0.04	0.152	0.004
	2.63	0.06	0.244	0.005

Table 1: Single-Sample Uncertainty Calculations for Filter Face Velocity and Reynolds Number

	Filter Face Velocity (m/s)	Multiple-Sample Uncertainty (m/s)	Reynolds Number	Multiple-Sample Uncertainty
Constant Output Atomizer	0.50	0.01	0.046	0.001
	1.50	0.01	0.139	0.001
	2.50	0.02	0.232	0.001
Fluidized Bed	0.65	0.01	0.0600	0.0004
	1.64	0.02	0.152	0.001
	2.63	0.03	0.244	0.002

Table 2: Multiple-Sample Uncertainty Calculations for Filter Face Velocity and Reynolds Number

4. Data

4.1 Collection Efficiency

Collection efficiency was calculated for each test condition. In this study, there were a total of six different test conditions. They included various combinations of Filtrete™ and neutralized Filtrete™ media with charged and uncharged NaCl particles. Additionally, Arizona road dust was tested, without separation of charged and uncharged particles, with both the Filtrete™ and neutralized Filtrete™ media. An average efficiency and standard deviation for each filter condition was calculated from 3 separate filter specimens. Each specimen consisted of 3 upstream and 2 downstream samples for each filter tested. Total

aerosol collection efficiency, E, was calculated according to the following equation (Liu & Lee, 1976):

$$E = 1 - \frac{\bar{C}_d}{\bar{C}_u}\left(\frac{\bar{P}_u}{\bar{P}_d}\right) \ . \qquad [17]$$

In equation [17], $\bar{C}$ is the average aerosol concentration (#/cm^3), $\bar{P}$ is the average air pressure, and the subscripts *u* and *d* indicate upstream and downstream of the filter, respectively. The pressure correction factor, $\left(\frac{\bar{P}_u}{\bar{P}_d}\right)$, accounts for downstream flow expansion from the filter pressure drop (Hubbard et al., 2012). Dilution in the downstream concentration can be significant under the studied air flow conditions in comparison to upstream concentration ($1.01 < \left(\frac{\bar{P}_u}{\bar{P}_d}\right) < 1.09$). In addition, the moving average of the total aerosol collection efficiency was calculated in order to smooth out small fluctuations in the data. In this study, efficiency data is presented separately according to the effects of filter face velocity and fiber charge. The four basic deposition mechanisms for aerosol particles to deposit onto the surface of a fiber will be discussed in detail in the following sections (Figure 15).

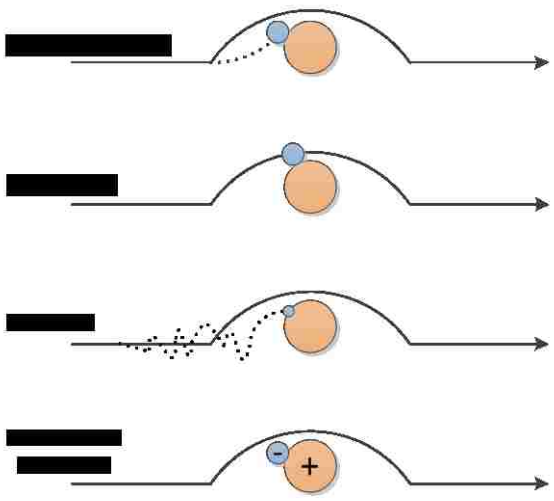

Figure 15: Four Basic Particle Deposition Mechanisms

4.2 Effects of Fiber Charge

4.2.1 Filter Collection Efficiency of Charged Media

Filtrete™ is a highly efficient filtration material with low pressure drop, characteristics which make it ideal for applications like respirators (Brown, 1993; Hinds, 1999; J. Kim et al., 2010; Wang, 2001). However, as face velocity increases, collection efficiency decreases due to shorter residence times associated with aerosol deposition by electrostatic attraction and diffusion (C. S. Kim et al., 2006). Filter collection efficiency of the Filtrete™ media with NaCl and ARD are presented in this section with associated standard deviations (Figure 16). Each aerosol was independently tested and neutralized to Boltzmann charge equilibrium at the exhaust of the aerosol generation reservoir with a bipolar ionizing device.

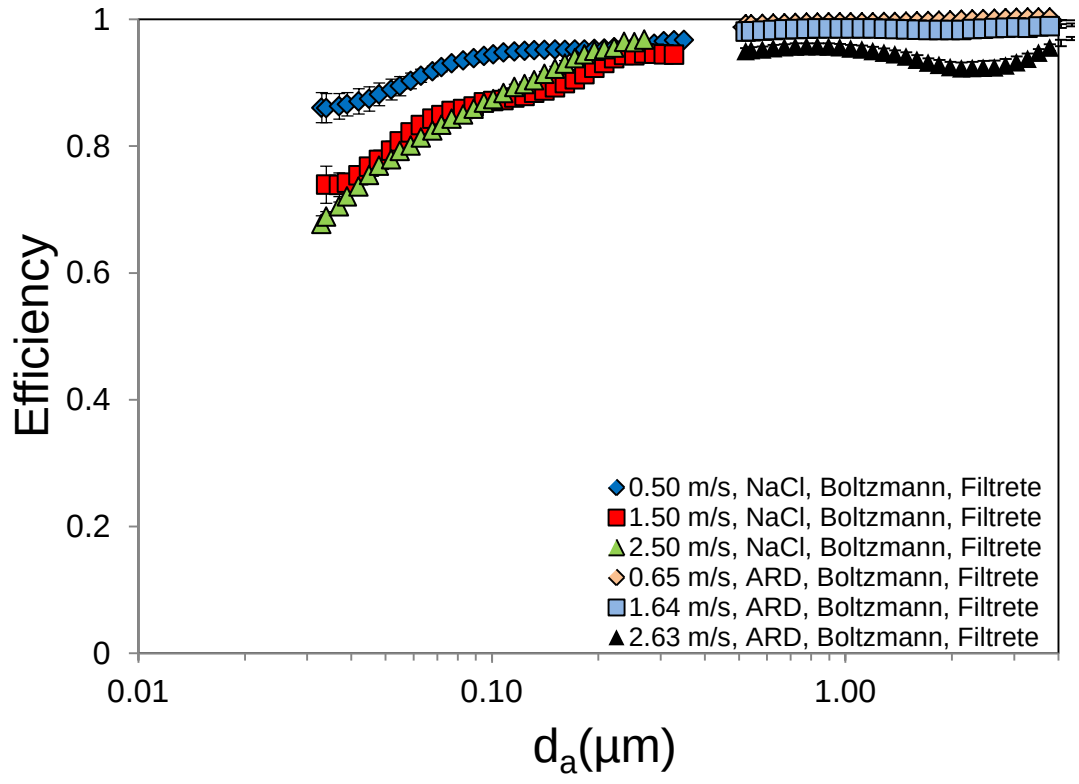

Figure 16: Effects of Fiber Charge with Charged Media

NaCl particles were generated and dispersed into the filter test bed system. System face velocities were 0.50 ± 0.01 m/s, 1.50 ± 0.03 m/s, and 2.50 ± 0.04 m/s. Under these conditions, particles were primarily separated from the air flow according to the following filtration mechanisms: diffusion, interception, and electrostatic attraction. Diffusion and interception are well characterized collection mechanisms (Hinds, 1999). Diffusion is the primary collection mechanism for particles smaller than 0.1 μm which is due to Brownian motion. Brownian motion is the random motion of particles due to collision with gas molecules. Because of this motion pattern, the likelihood of collision with filter fibers increases (Figure 15). Interception happens when a particle follows a gas streamline and comes into contact to the surface of a fiber that is within one particle radius (Hinds, 1999).

Although competing collection mechanisms can be present at the same time, each is most effective in different size ranges. For this reason, all filters have a particle size range with a minimum collection efficiency. (Hinds, 1999; Wang, 2001). Under current conditions, however, electrostatic attraction, specifically Coulombic force, was particularly important. This force is the attraction that two bodies experience when oppositely charged. In this case, the Filtrete^{TM} media was both positively and negatively charged in different regions of the fiber surface and attracted NaCl particles which possessed the Boltzmann charge equilibrium distribution. Electrostatic effects caused filter efficiency to increase within minimum efficiency size range However, as filter face velocity increased from 0.5 to 2.5 m/s, the amount of time each particle had to interact with the Filtrete^{TM} media decreased and decreased collection efficiency, as seen in Figure 16. This is because the convective velocity due to air flow becomes higher as velocity increases, decreasing the time the particle has to come into contact with the surface of the fiber due to drift velocity, Figure 17 (Brown, 1993).

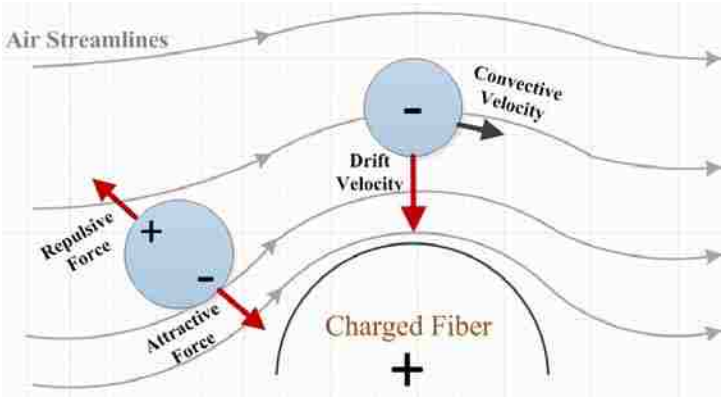

Figure 17: Schematic of a Charged and Neutral Particles Captured by a Charged Fiber

In addition, Arizona road dust (ARD) was dispersed into the filter test bed system separately from the NaCl particles. System filter face velocities in this case were 0.65 ± 0.03 m/s, 1.64 ± 0.04 m/s, and 2.63 ± 0.06 m/s. ARD particles are larger in comparison to NaCl particles and are primarily collected by interception, inertial impaction, and Coulombic force. Inertial impaction occurs when the momentum of the particle cannot adjust to abruptly changing streamlines around a fiber and hits the fiber, Figure 17 (Hinds, 1999). Impaction can increase according to various conditions: greater particle inertia or a more abrupt curvature of streamlines from a smaller fiber size (Hinds, 1999).

The collection efficiency was nearly 100%, which was due to the three mechanisms described. However, in Figure 16, the filter face velocity at 2.63 m/s had a slight dip in efficiency starting around 0.7 μm. It is speculated that this was due to particle bounce. When particles come into contact with a fiber by inertial impaction, there is a chance that the particle velocity will overcome the adhesion to the fiber surface, which is called particle bounce (Brown, 1993). It seems as though the adhesion affects, possibly due to the Coulombic force from the Filtrete^{TM} media, were strong enough to retain the particles at 0.65 and 1.64 m/s.

Filter efficiency was plotted as a function of filter face velocity for a selected number of aerodynamic diameters, Figure 18. Only NaCl particles will be discussed because of their well-known properties. At the smallest particle diameter (0.04 μm) collection efficiency decreases as filter face velocity increases because at higher convective velocity the NaCl particles have less time to drift toward the charged fibers. In addition, diffusion is inversely based on Peclet number (Pe), defined as

$$Pe = \frac{d_f V}{D_p} \; . \qquad [19]$$

So, as filter face velocity increases, diffusional collection also decreases. In this case, the effects of electrostatic attraction and diffusion act in similar ways, i.e. lower efficiency at higher filter face velocities.

As particle diameter increases inertial impaction begins to aid in collection efficiency at higher filter face velocities. Inertial impaction can be assessed with the Stokes number (Stk), defined as

$$Stk = \frac{\rho_p d_p^2 C_c V}{18 \eta d_f} \; . \qquad [19]$$

Although the effect of electrostatic attraction diminishes due to an increase in filter face velocity, as particle diameter increases, collection efficiency will improve due to inertial impaction. Eventually, inertial impaction will become the dominant collection mechanism with larger particles at higher filter face velocities, as seen at 2.5 m/s and d_a = 0.30μm.

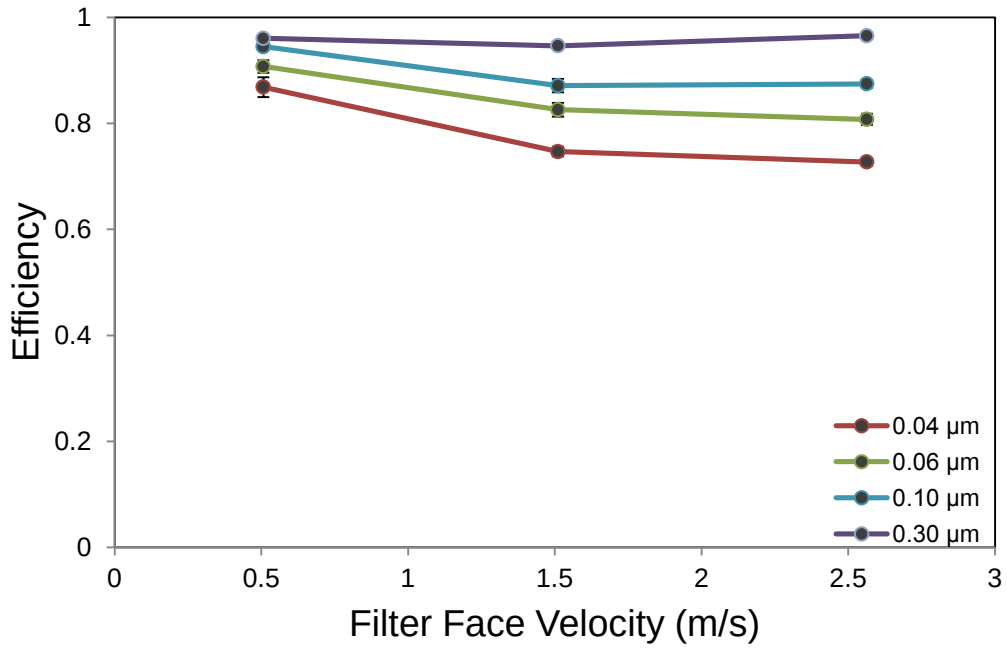

Figure 18: Effect of Filter Face Velocity for NaCl Particles at Different Diameters

4.2.2 Filter Collection Efficiency of Neutralized Filter Media

Similar tests were conducted using the same conditions presented in section 4.2.1, however, the Filtrete™ media was neutralized to eliminate fiber charge. As was discussed in section 3.2.2, each filter was soaked in isopropanol for 1 hour and allowed to dry for 24 hours to ensure neutralization. In previous studies, this has been seen to significantly, if not completely, eliminate fiber charge (Hinds, 1999; Huang et al., 2007; J. Kim et al., 2010; Martin & Moyer, 2000). Filter collection efficiency of the neutralized Filtrete™ media with NaCl and ARD are presented in this section with associated standard deviations (Figure 19). Each aerosol was independently tested and neutralized to the Boltzmann charge equilibrium distribution at the exhaust of the aerosol reservoir with an ionizing device.

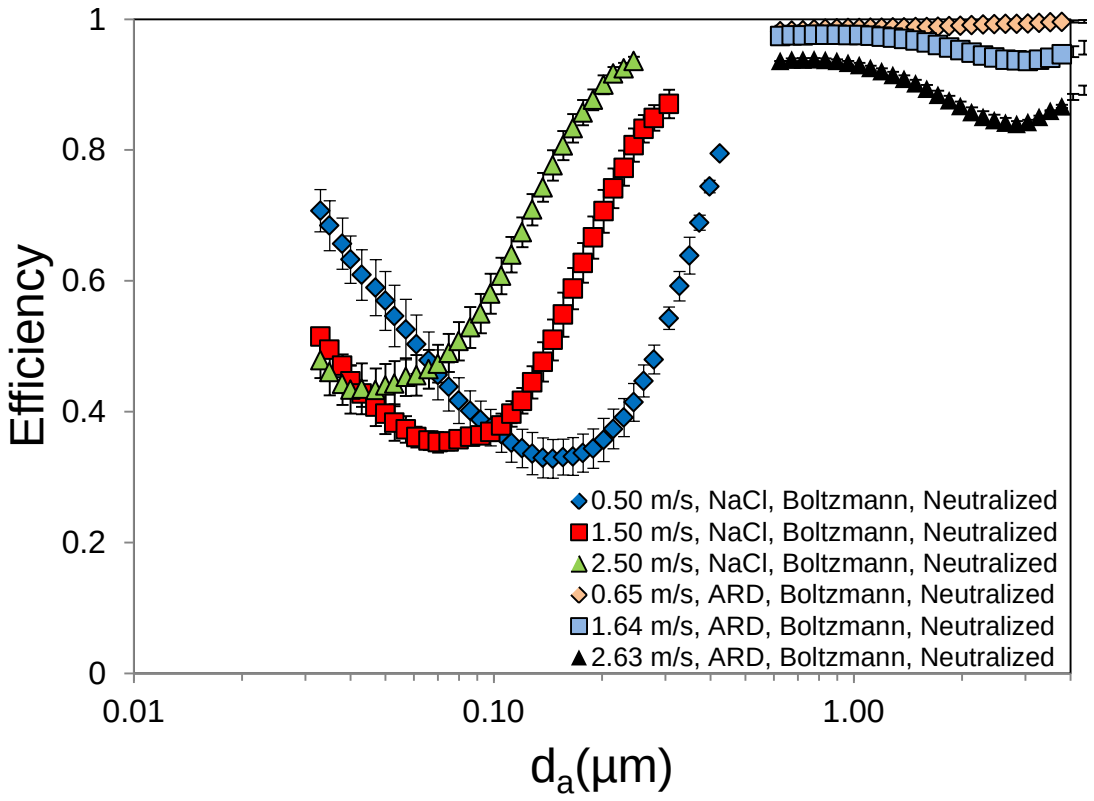

Figure 19: Effects of Fiber Charge with Neutralized Media

NaCl particles were generated and dispersed into the filter test bed system. The system face velocities were 0.50 ± 0.01 m/s, 1.50 ± 0.03 m/s, and 2.50 ± 0.04 m/s. The primary collection mechanisms were diffusion, interception, and inertial impaction. Comparing Figures 16 and 19, it is evident that there is a significant decrease in efficiency for all three filter face velocities. The most significant decrease was seen at about 0.15 µm at a filter face velocity of 0.5 m/s, where collection efficiency dropped from about 95% to 33%. This indicates that Coulombic force was a significant mechanism for particle collection within this region.

In Figure 19, Brownian diffusion was the main collection mechanism for particles <0.1 µm, which is seen in the left-hand tails of the NaCl curves. The minimum collection efficiency, from 0.03-0.3 µm, is within a range where competing forces are at their lowest.

This is because competing mechanisms are most effective at different size ranges and all filters have a particle size where collection efficiency is at a minimum (Hinds, 1999; Wang, 2001). Within this range, diffusion, interception, and inertial impaction, collectively, are at their lowest efficiency. Additionally, there is a noticeable shift of collection efficiency as face velocity increased from 0.50 to 2.50 m/s. This was due to inertial impaction. As inertia increases, there is a higher chance aerosol particles will impact the surface of the fiber. This noticeable shift is an increase in inertial separation (Hubbard et al., 2012).

ARD was dispersed into the filter test bed system separately from the NaCl particles. The system filter face velocities in this case were 0.65 ± 0.03 m/s, 1.64 ± 0.04 m/s, and 2.63 ± 0.06 m/s. The main mechanisms for particle collection within this particle size range were interception and inertial impaction. When comparing Figures 16 and 19, it is apparent that Coulombic force increased collection efficiency of the Filtrete^{TM} media. Electrostatic force makes adhesion more likely (Brown, 1993). When the Filtrete^{TM} media was neutralized, it increased the possibility of particle bounce. As filter face velocity increased, particle bounce increased because of the added particle kinetic energy and decrease in adhesion.

Filter efficiency was plotted as a function of filter face velocity for a selected number of aerodynamic diameters, Figure 20. Once again, only NaCl particles will be discussed because of their well-known properties. Because the Filtrete^{TM} media is neutralized, it is presumed that electrostatic attraction is negligible. The collection mechanism that describes particle collection of small particles is diffusion which is based on Brownian motion. Diffusion is the only collection mechanism that increases as particle diameter decreases because it is inversely based on Peclet number. In Figure 20, collection efficiency decreases at all three filter face velocities for the smallest particle size (0.04μm). This is because the

dominant collection mechanism at this particle size is diffusion. However, as particle size increases (0.06µm) collection efficiency decreases with filter face velocity until inertial impaction shifts and begins to be the dominate collection mechanism at 2.5 m/s. At the particle size of 0.10µm, diffusion becomes less efficient at 0.5 m/s while at higher filter face velocity collection efficiency increases due to inertial impaction. By 0.15µm to 0.30µm, the influence of diffusion is negligible while inertial impaction has increased collection efficiency due to an increase in Stokes number.

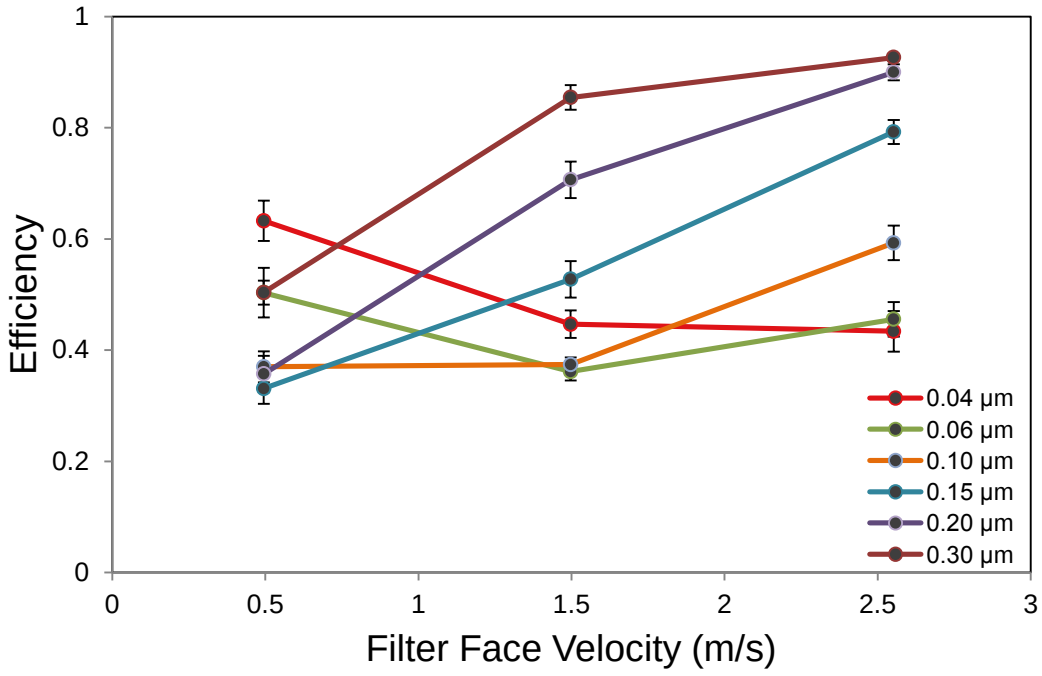

Figure 20: Effect of Filter Face Velocity on NaCl Particles at Different Diameters

4.3 Effect of Electrostatic Attraction at Fixed Filter Face Velocities

The effect of filter face velocity was analyzed in detail for both the Filtrete™ and neutralized Filtrete™ media at 0.50, 1.50, and 2.50 m/s. The remainder of this work focuses on NaCl particles because of their well-known properties (e.g., density and shape factor) and precision of experimental data. Collection efficiency was calculated according to equation

[17]. Particles were generated using the TSI Constant Output Atomizer discussed in Section 2. NaCl particles were tested in both Boltzmann charge equilibrium and zero charge states. As was discussed in section 2.1, zero charge NaCl particles were generated by removing all charged NaCl particles with an electrostatic precipitator (ESP) designed for this study. However, due to the electrostatic precipitator, particles with aerodynamic diameters (d_a) of about 0.3µm or larger were nearly all removed and will not be shown in the graphs below. It was important to compare the electrostatic force under various conditions at the same velocity, in order to determine the full effect of this collection mechanism.

4.3.1 Filter Face Velocity of 0.5 m/s

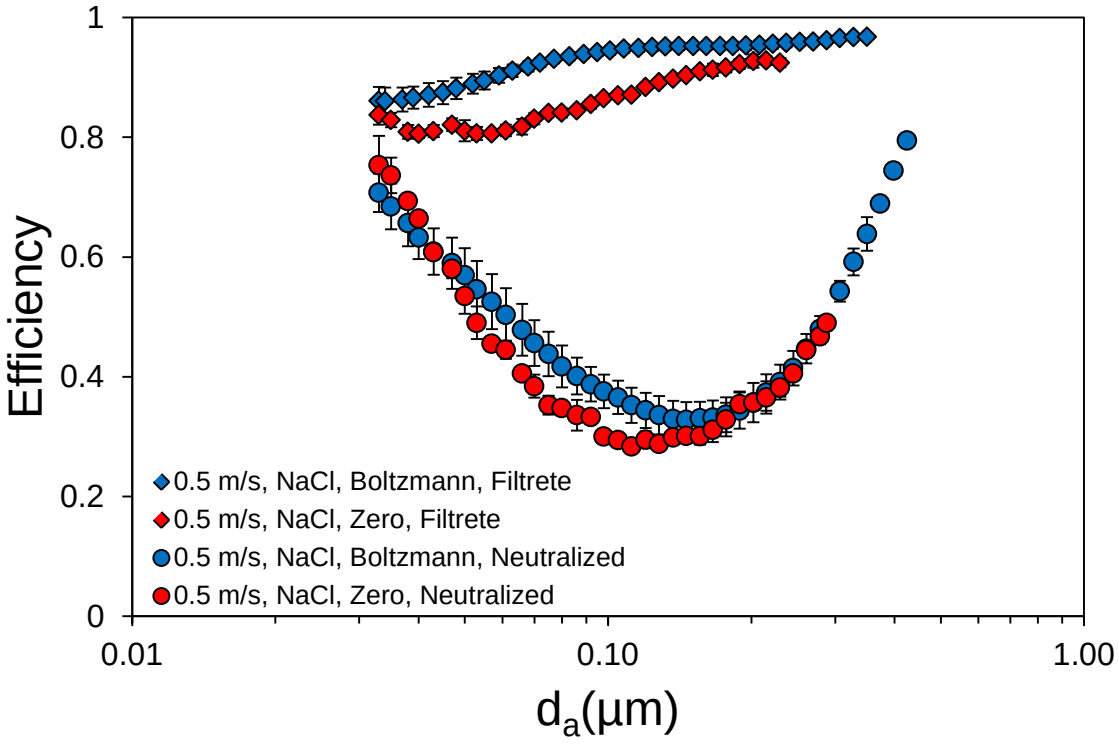

Figure 21: Effect of Electrostatic Attraction at a Fixed Filter Face Velocity of 0.50 m/s

The filter face velocity of the system was set at 0.50 ± 0.01 m/s. The effect of the Filtrete™ media and charge particles will be discussed first. Overall, filtration was most

efficient under Coulombic force, where Filtrete™ media was charged and NaCl particles were at the Boltzmann charge distribution, Figure 21. Under these conditions, drift velocity is at its highest, increasing the likelihood that the particles will overcome the convective velocity of the air streams to reach the surface of the Filtrete™ media, Figure 17. This media was also tested with zero charged particles. Collection efficiency, using zero charged particles, was nearly as high as Coulombic force due to polarization force. Under the influence of the polarization force, a dipole is induced in a neutral particle by the electric field of the fiber, attracting the neutral particle to the charged fiber, Figure 17 (Brown, 1993). Although efficiency was not as high as Coulombic force, collection efficiency, seen in Figure 21, indicates that fiber charge has a significant impact on collection even when charged particles were removed.

The Filtrete™ media was neutralized and tested under similar conditions to above. Collection efficiency significantly decreased due to neutralization of the Filtrete™ media for NaCl particles under zero charge and Boltzmann charge equilibrium. With the absence of electrostatic forces, which was the case with zero charged particles and a neutralized filter, traditional collection mechanisms (diffusion, interception, and inertial impaction) govern collection efficiency, as was discussed in section 4.2.2. Under the influence of image force, a dipole is formed by a neutral fiber due to a charged particle, causing electrostatic attraction. This could have been the case with the neutralized Filtrete™ media and Boltzmann charge distributed NaCl particles. However, in Figure 21, image force appears not to have a significant impact on collection efficiency in this study. When comparing the two neutralized Filtrete™ curves, average efficiencies are within experimental standard deviation. If image

force effects were important, it is presumed that efficiency, with respect to the condition where electrostatic forces were removed, should have been higher.

4.3.2 Filter Face Velocity of 1.50 m/s

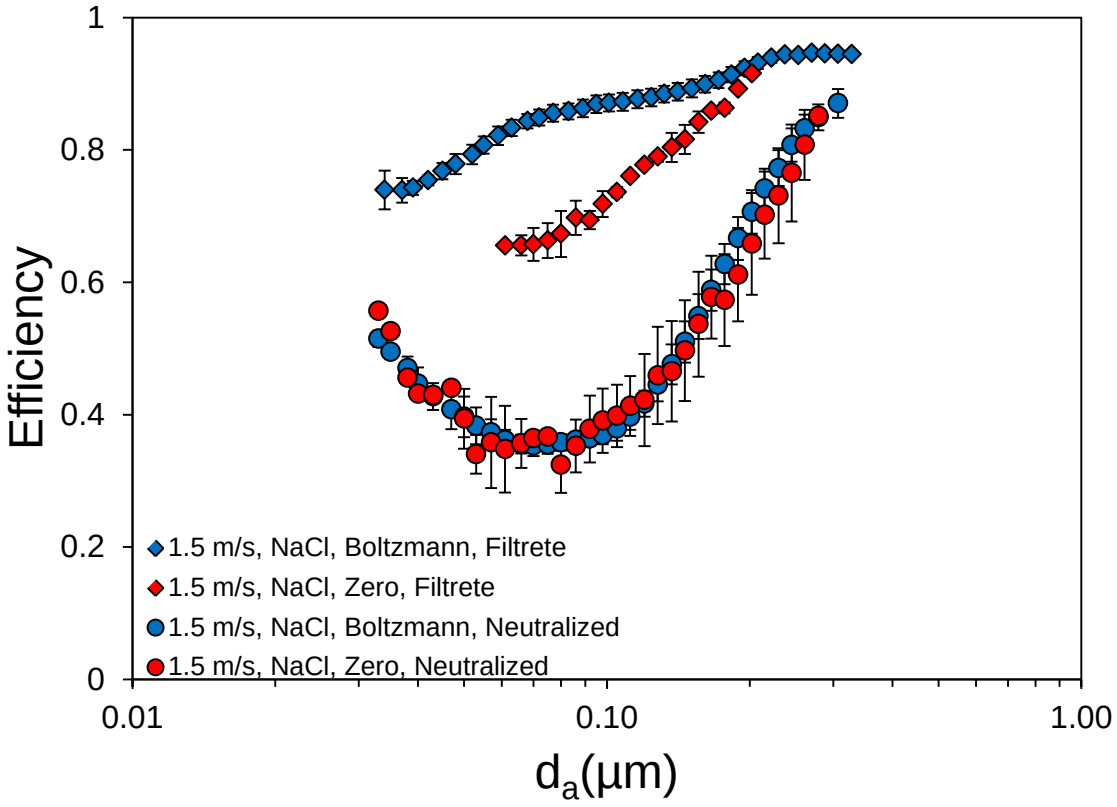

Figure 22: Effect of Electrostatic Attraction at a Fixed Filter Face Velocity of1.50 m/s

As filter face velocity was increased from 0.5 m/s to 1.50 m/s, there was a noticeable difference in efficiency, Figure 22. As was discussed in section 4.2.1, as filter face velocity increases, collection efficiency decreases due to a shorter residence time associated with aerosol deposition by electrostatic attraction and diffusion (C. S. Kim et al., 2006). Coulombic and polarization force were both affected by the increase in filter face velocity. However, the polarization force was less efficient at particle separation for lower aerodynamic diameters than the Coulombic force. Although an induced dipole is still created

within the particle due to polarization, the increase in convective velocity causes an increase in fiber penetration, Figure 17. As filter face velocity increased, this difference in efficiency became more apparent between the two electrostatic forces.

When the Filtrete^{TM} media was neutralized and run under the same conditions above, there was a noticeable increase in efficiency due to inertial impaction, Figure 22. As was discussed in section 4.2.2, as filter face velocity increases, the probability that a particle impacts the fiber surface increases. This phenomenon shifts the collection efficiency curves up and to the left. It is also seen in Figure 20 that the image force due to particle induced fiber charge, is once again negligible.

4.3.3 Filter Face Velocity of 2.50 m/s

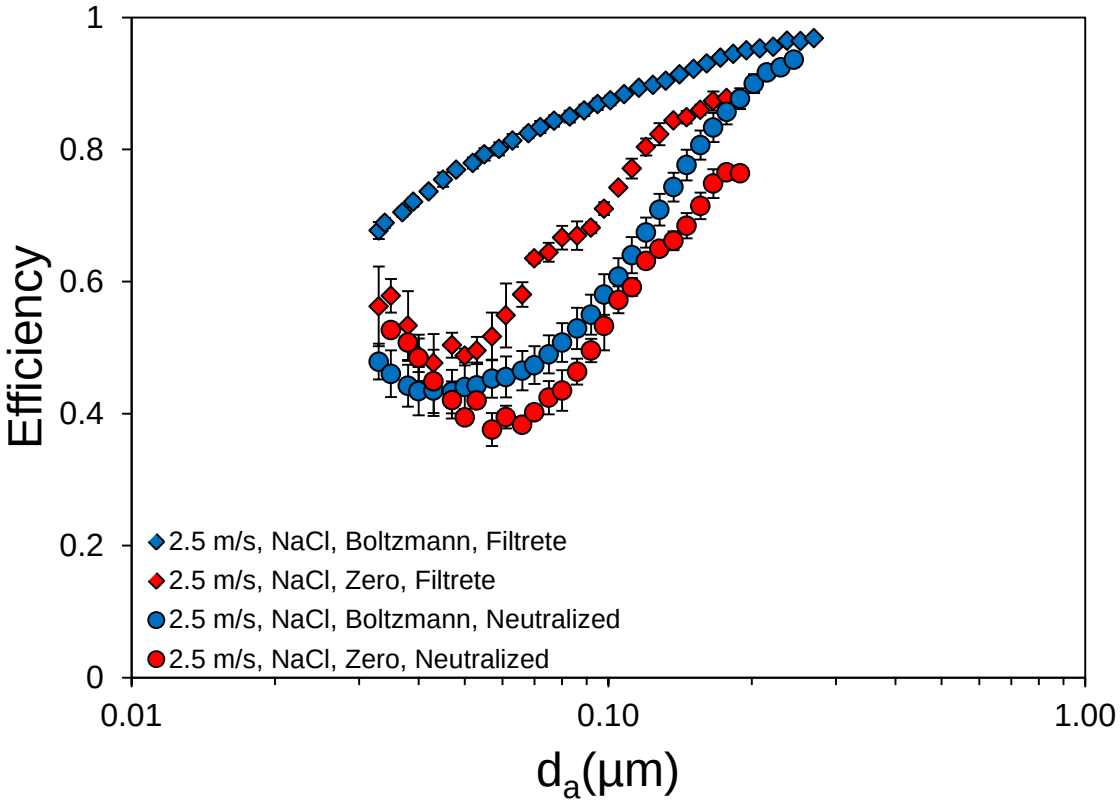

Figure 23: Effect of Electrostatic Attraction at a Fixed Filter Face Velocity of 2.50 m/s

As filter face velocity increased from 1.50 to 2.50 m/s, there was a noticeable difference in collection in comparison to Figure 22. The electrostatic separation effects due to Coulombic and polarization force are less efficient in comparison to Figures 21 and 22. Additionally, the collection efficiency curve which represents the polarization effect nearly overlapped with the two neutralized Filtrete^{TM} media curves within 10%. This shows that electrostatic attraction due to polarization is becoming less important while collection due to inertial impaction is becoming more important. This showed that although electrostatic attraction from a charged filter media can significantly increase collection efficiency at lower face velocities, it does have its limitations as velocity increases.

5. Discussion

The data presented in this study are unique because they are outside the realm of contemporary filtration theory where the theory is incomplete, making the electrostatic effects difficult to characterize without direct measurements. At present, there is minimal experimental data and little to no numerical work conducted within this flow regime. Filtration mechanisms describing particle collection efficiency have been studied extensively. These include diffusion, interception, and inertial impaction (Hinds, 1999). However, most theories that model these filtration mechanisms have limitations. Kuwabara described the flow field through an array of staggered fibers, often called the cell model, analytically by neglecting the inertial terms in the Navier-Stokes equation (Kuwabara, 1959). However, as air velocity increases, the inertial force becomes more important and must be taken into consideration. The contemporary single fiber efficiency models described by Hinds assume viscous flow, $Re_f << 1$, where the Kuwabara cell model has been applied in their development. The advantage of using single fiber efficiency is that it is independent of filter

thickness and solidity, making it a universal parameter and easier to compare two different filters. However, it is important to note that although a filter could have a lower single fiber efficiency in comparison to another filter, total efficiency of the same filter may be higher because of filter thickness (Baron & Willeke, 2001). Unfortunately, the accuracy of single fiber efficiency models becomes questionable as viscous flow begins to transition to an inertial flow at $Re_f \geq 0.1$ (Hinds, 1999). In this study, at $Re_f = 0.05$, filtration theory holds because Reynolds number was small, however, as Reynolds number increased the viscous flow assumption is questionable, therefore, performance needed to be measured.

Electrostatic attraction forces, i.e. Coulombic, polarization, and image forces, have been described well by Brown (1993). One of the key parameters of his models was fiber charge density. However, many studies have found it very difficult to quantify due to a lack of experimental methods. From literature, fiber charge density has varied from 1.00×10^{-10} to 3.42×10^{-8} C/m (Huang et al., 2007; Kanaoka, Emi, Otani, & Iiyama, 1987; Lathrache & Fissan, 1987; Sae-lim, Tanthapanichakoon, & Kanaoka, 2006; Wang, 2001). Because of this discrepancy, this parameter is often back calculated from overall filter efficiency. Therefore, accurate predictions of filter efficiency require experimental measurements. Fjeld (1988) suspected that lack of agreement could be that fiber charge could have been lost between production and when the experiment was run. Another possibility was that the fibers could have been discharged during the experiment (Fjeld & Owens, 1988). Although he dismissed this latter possibility, it has been seen that electret media can lose efficiency due to exposure to filter loading and atmospheric, secondary, or organic aerosols (J. Kim et al., 2010; Martin & Moyer, 2000; Wang, 2001). Unfortunately, little is known exactly why fiber neutralization

occurs when charged fibers come into contact with organic solvents; therefore, further research is needed.

6. Summary

Aerosol collection efficiency was measured at nontraditional filter face velocities ranging from 0.5 to 2.5 m/s, conditions representative of high volume sampling. Filtrete™ from the 3M™ company was used in this study and has been seen to significantly increase particle collection efficiency due to the presence of electrostatically charged fibers. As filter face velocity increased particle collection efficiency of the charged fibers decreased. This media was tested against test aerosols of sodium chloride and Arizona road dust in a specifically designed high velocity filter test bed system at filter face velocities of 0.5, 1.5, and 2.5 m/s, a pressure of 0.8 atm, and temperature of 20°C. This range of conditions gave approximate Reynolds numbers ranging from 0.05-0.24, where filtration theory is incomplete and does not predict performance of electret media. Total collection efficiency was measured, since very little experimental evidence exists in this regime.

In order to study the electrostatic efficiency of the Filtrete™ media within this regime, measurements were taken with and without electrostatically charged fibers and particles. Similar to other studies in the literature, charged fibers were neutralized using isopropanol and allowed to dry. As filter face velocity increased, collection efficiency of the charged Filtrete™ media decreased in all cases. However, the collection efficiency of the neutralized media increased due to an increase in inertial impaction and shift in the diffusion regime for particles $d_a \leq 400$ nm. Particle bounce was seen with both charged and neutralized media for particles $d_a \geq 400$ nm as filter face velocity increased, though particle

bounce was less pronounced with the charged fibers due to electrostatic attraction which was thought to aid in particle retention.

Total electrostatic attraction was also analyzed, which included the effects of Coulombic, polarization, and image forces. The collection efficiency of Filtrete^{TM} media was characterized with both charged and neutralized fibers, and particles in Boltzmann charge distribution or zero charge. Data were compared at equal filter face velocity. Coulombic forces had the most significant effect on collection efficiency at all filter face velocities, followed by conditions under the effects of the polarization force. However, as filter face velocity increased, there was a noticeable decrease in collection efficiency, especially with conditions where the polarization force was responsible for filtration. As convective velocity increased, particles had less time to drift toward the electrostatically charged fibers decreasing collection efficiency. In addition, the data showed a shift in dominant collection mechanisms as filter face velocity increased. At 2.5 m/s, the effect of electrostatic attraction decreased in collection efficiency while inertial impaction increased. The effects of the image force were negligible at all filter face velocities.

In this study, the effect of electrostatic attraction was optimal at lower filter face velocities and smaller particles sizes where minimum collection regions exist. What it also showed was while the effect of electrostatic attraction decreased due to an increase in filter face velocity, collection efficiency due to inertial impaction increased. This meant that at higher filter face velocities, electrostatic attraction would no longer be the dominant collection mechanism. This study provides unique empirical data outside of the viscous filter flow regime, data which is useful in the design of, and performance prediction of, high volume commercial and industrial applications, such as HVAC systems, air craft sampling,

and ground based sampling. The data presented can be used to “validate” numerical models for filtration at moderate Reynolds numbers, where data is scarce and traditional filtration theory is incomplete. Additional research is needed to understand the fundamental principles of electret neutralization with organic solvents.

References

3M. (1993). Comparison of 3M Filtrete Media with TEBF Media *Technical Report*. St. Paul, MN USA.

Baron, P. A., & Willeke, K. (2001). *Aerosol Measurement - Principles, Techniques, and Applications (2nd Edition)*: John Wiley & Sons.

Barrett, L. W., & Rousseau, A. D. (1998). Aerosol Loading Performance of Electret Filter Media. *American Industrial Hygiene Association Journal, 59*(8), 532-539. doi: 10.1080/15428119891010703

Bragg, G. M., & Pearson, B. M. (1979). A Model of Aerosol Filtration by Fibrous Filters. *Industrial & Engineering Chemistry Process Design and Development, 18*(1), 171-177. doi: 10.1021/i260069a024

Brown, R. C. (1993). *Air Filtration: An Integrated Approach to the Theory and Applications of Fibrous Filters* (1st ed.). New York, USA: Pergamon Press.

Cohen, B. S., Xiong, J. Q., Fang, C.-P., & Li, W. (1998). Deposition of Charged Particles on Lung Airways. *Health Physics, 74*(5), 554-560.

DeCarlo, P., Slowik, J., & Worsnop, D. (2004). Particle Morphology and Desnity Characterization by Combined Mobility and Aerodynamic Diameter Measurements. Part 1: Theory. *American Association for Aerosol Research, 38*, 1185-1205.

Fjeld, R. A., & Owens, T. M. (1988). The Effect of Particle Charge on Penetration in an Electret Filter. *Ieee Transactions on Industry Applications, 24*(4), 725-731.

Henry, F., & Ariman, T. (1981). Cell model of aerosol collection by fibrous filters in an electrostatic field. *Journal of Aerosol Science, 12*(2), 91-103. doi: 10.1016/0021-8502(81)90041-0

Hinds, W. C. (1999). *Aerosol Technology: Properties, Behavior, and Measurement of Airborne Particles* (2nd ed.). New York, USA: John-Wiley & Sons. Inc.

Huang, S.-H., Chen, C.-W., Chang, C.-P., Lai, C.-Y., & Chen, C.-C. (2007). Penetration of 4.5nm to 10um aerosol particles through fibrous filters. *Journal of Aerosol Science, 38*(7), 719-727. doi: 10.1016/j.jaerosci.2007.05.007

Hubbard, J. A., Brockmann, J. E., Dellinger, J., Lucero, D. A., Sanchez, A. L., & Servantes, B. L. (2012). Fibrous Filter Efficiency and Pressure Drop in the Viscous-Inertial Transition Flow Regime. *Aerosol Science and Technology, 46*(2), 138-147. doi: Doi 10.1080/02786826.2011.616555

Kanaoka, C., Emi, H., Otani, Y., & Iiyama, T. (1987). Effect of Charging State of Particles on Electret Filtration. *Aerosol Science and Technology, 7*(1), 1-13. doi: 10.1080/02786828708959142

Kim, C. S., Bao, L., Okuyama, K., Shimada, M., & Niinuma, H. (2006). Filtration efficiency of a fibrous filter for nanoparticles. [Article]. *Journal of Nanoparticle Research, 8*(2), 215-221. doi: 10.1007/s11051-005-9017-x

Kim, J., Jasper, W., Barker, R. L., & Hinestroza, J. P. (2010). Application of Electrostatic Force Microscopy on Characterizing an Electrically Charged Fiber. *Fibers and Polymers, 11*(5), 775-781. doi: DOI 10.1007/s12221-010-0775-4

Kline, S. J., & McClintock, F. A. (1953). Describing Uncertainties in Single-Sample Experiements. *Mechanical Engineering, 75*(1).

Kuwabara, S. (1959). THE FORCES EXPERIENCED BY RANDOMLY DISTRIBUTED PARELLEL CIRCULAR CYLINDERS OR SPHERES IN A VISCOUS FLOW AT SMALL REYNOLDS NUMBERS. [Article]. *Journal of the Physical Society of Japan, 14*(4), 527-532. doi: 10.1143/jpsj.14.527

Lathrache, R., & Fissan, H. (1987). Enhancement of Particle Deposition in Filters due to Electrostatic Effects. *Filtration and Sparation, 24*(6), 418-422.

Lee, M., Otani, Y., Namiki, N., & Emi, H. (2002). Prediction of collection efficiency of high-performance electret filters (vol 35, pg 57, 2002). [Correction]. *Journal of Chemical Engineering of Japan, 35*(9), 922-922.

Liu, B. Y. H., & Lee, K. W. (1976). Efficiency of membrane and nuclepore filters for submicrometer aerosols. *Environmental Science & Technology, 10*(4), 345-350. doi: 10.1021/es60115a002

Martin, S. B. J., & Moyer, E. S. (2000). Electrostatic Respirator Filter Media: Filter Efficiency and Most Penetrating Particle Size Effects. *Applied Occupational and Environmental Hygiene, 15*(8), 609-617.

Sae-lim, W., Tanthapanichakoon, W., & Kanaoka, C. (2006). Correlation for the efficiency enhancement factor of a single electret fiber. *Journal of Aerosol Science, 37*(2), 228-240. doi: 10.1016/j.jaerosci.2005.05.001

Shaffer, R., & Rengasamy, S. (2009). Respiratory protection against airborne nanoparticles: a review. *Journal of Nanoparticle Research, 11*(7), 1661-1672. doi: 10.1007/s11051-009-9649-3

Spencer, M. T., Shields, L. G., & Prather, K. A. (2007). Simultaneous Measurement of the Effective Density and Chemical Composition of Ambient Aerosol Particles. *Environmental Science & Technology, 41*(4), 1303-1309. doi: 10.1021/es061425+

TSI. (2002). Model 3321 Aerodynamic Particle Sizer Spectrometer: Instruction Manual (Revision D ed.). St. Paul, MN USA: TSI Inc.

TSI. (2003). Model 3936 SMPS (Scanning Mobility Particle Sizer): Instruction Manual (Revision H ed.). Shoreview, MN USA: TSI, Inc.

TSI. (2005). Model 3076 Constant Output Atomizer: Instruction Manual (Revision J ed.). Shoreview, MN USA: TSI Inc.

Wang, C.-S. (2001). Electrostatic forces in fibrous filters—a review. *Powder Technology, 118*(1–2), 166-170. doi: 10.1016/s0032-5910(01)00307-2

Wei, J., Chun-Shun, C., & Cheong-Ki, C. (2006). the Aerosol Penetration Through an Electret Fibrous Filter. *Chinese Physics, 15*(8), 1009-1963.